IN-VIVO EVIDENCE FOR INCREASED TAU DEPOSITION IN TEMPORAL LOBE EPILEPSY

Raúl R. Cruces[1], Jack Lam[1], Thaera Arafat[1], Jessica Royer[1], Judy Chen[1], Ella Sahlas[1], Arielle Dascal[1], Raluca Pana[2], Robert Hopewell[1], Chris Hung-Hsin Hsiao[1], Gassan Massarweh[1], Jean-Paul Soucy[1], Sylvia Villeneuve[3], Lorenzo Caciagli[4,5], Matthias J. Koepp[4], Andrea Bernasconi[1], Neda Bernasconi[1], Boris C. Bernhardt[1*].*

1. McConnell Brain Imaging Centre, Montreal Neurological Institute, McGill University, Montreal, Québec, Canada.
2. Montreal Neurological Institute, McGill University Health Centre (MUHC) and other McGill University
3. StoP-AD Centre, Douglas Mental Health University Institute, McGill University, Montréal, QC, Canada
4. UCL Queen Square Institute of Neurology, University College London, London WC1N 3BG, UK
5. Department of Neurology, Inselspital, Sleep-Wake-Epilepsy Center, Bern University Hospital, University of Bern, Bern, Switzerland

** joint senior authors*

Corresponding author
Raul Cruces, PhD
raul.rodriguez-cruces@mcgill.ca

Boris C. Bernhardt, PhD
boris.bernhardt@mcgill.ca

GLOSSARY:

TLE = temporal lobe epilepsy. **PET** = positron emission tomography. **MRI** = magnetic resonance imaging. **NI** = neuroinflammation

KEYWORDS:

Temporal lobe epilepsy | [^{18}F]MK-6240 | tauopathy | neuroimaging | neuroinflammation

SHORT TITLE:

Increased *in-vivo* tau in TLE

ABSTRACT

Temporal lobe epilepsy (TLE), the most common pharmaco-resistant epilepsy in adults, has been linked to structural brain changes extending beyond the mesiotemporal areas. While not traditionally viewed as a neurodegenerative disorder, recent *ex-vivo* studies have shown elevated levels of misfolded tau protein in TLE. This study investigated tau deposition in TLE patients using the *in-vivo* PET tracer [18F]MK-6240. 18 TLE patients and 20 healthy controls underwent PET imaging, with data analyzed to assess tau uptake and its relationship with brain connectivity, clinical variables, and cognitive function. Compared to controls, TLE patients exhibited markedly increased [18F]MK-6240 uptake in bilateral superior and medial temporal regions and the parietal cortex, with tau accumulation following regional functional and structural connectivity, disease duration, and cognitive impairment. These findings suggest that tau accumulation may contribute to the progression of TLE and cognitive decline, supporting a potential role of tau in epilepsy-related neurodegeneration.

INTRODUCTION

Mounting evidence suggests that temporal lobe epilepsy (TLE), the most common pharmaco-resistant epilepsy in adults, is not a static condition, but one that is associated with progressive changes extending beyond the mesiotemporal disease epicenter [1–4]. Although the exact causes of disease progression remain unknown, several lines of evidence suggest similar mechanisms as in Alzheimer's disease (AD), an established neurodegenerative condition. First, cognitive profiles in middle-aged pharmaco-resistant epilepsy patients resemble those of mild cognitive impairment, which can be linked to AD [5]. Furthermore, epidemiological studies have indicated an elevated risk for pharmaco-resistant epilepsy patients to be diagnosed with AD, and *vice versa* [6,7]. Across all age groups, patients with AD show a 3-fold higher risk of suffering from epilepsy [8,9]. Finally, an analysis of *ex-vivo* specimens in operated TLE patients has shown highly elevated levels of misfolded tau protein in operated TLE patients [10], a hallmark of AD pathology[11]. Such findings complement data from animal models of TLE, which demonstrate that seizure activity triggers tau hyperphosphorylation and amyloidogenic pathways [12,13].

Whole-brain patterns remain unknown due to limits imposed by the scope of resection. Also, while *ex-vivo* tau increases in TLE were related to postoperative cognitive decline [14], correlations with measures of preoperative cognitive function remain incompletely understood. These considerations underscore the need for *in-vivo* analyses of tau in TLE to evaluate its potential role as both a modulator of cognitive function and a predictor of clinical outcomes. Research in AD and other neurodegenerative conditions has benefitted from the introduction of second-generation PET tracers that are sensitive and specific to pathological deposits. In particular, the [^{18}F]-MK-6240 tracer (*henceforth* MK-6240) has shown high affinity and selectivity to intracellular neurofibrillary tangles [15–17]. In contrast, while there is an extensive PET literature in epilepsy on presurgical localization of hypometabolism via [^{18}F]fluorodeoxyglucose [18,19], PET studies in epilepsy have so far not systematically investigated tau tracers[7]. As such the whole brain distribution of tau in epileptic patients remains unknown. Unlike research in AD, where tau uptake patterns are increasingly understood and contextualized with respect to patterns of brain connectivity, there have not been any systematic assessments of potential network-level effects underlying the accumulation of these pathological deposits in TLE.

The objective of our study was to investigate the distribution and prevalence of tau aggregates in TLE using *in-vivo* MK-6240 PET. Tau mapping was complemented with network decoding models informed by multimodal MRI investigations in the same participants that tested for spatial associations of tau uptake in patients with patterns of global and local connectivity. Moreover, linear models examined associations with cognitive function assessed outside the scanner and clinical measures from the patients presurgical examination.

RESULTS

Widespread increases in tau uptake in TLE

Global mean MK-6240 SUVR was increased in patients with TLE relative to controls, both ipsilateral (t=2.36, p=0.02) and contralateral (t=2.75, p=0.008) to the seizure focus.

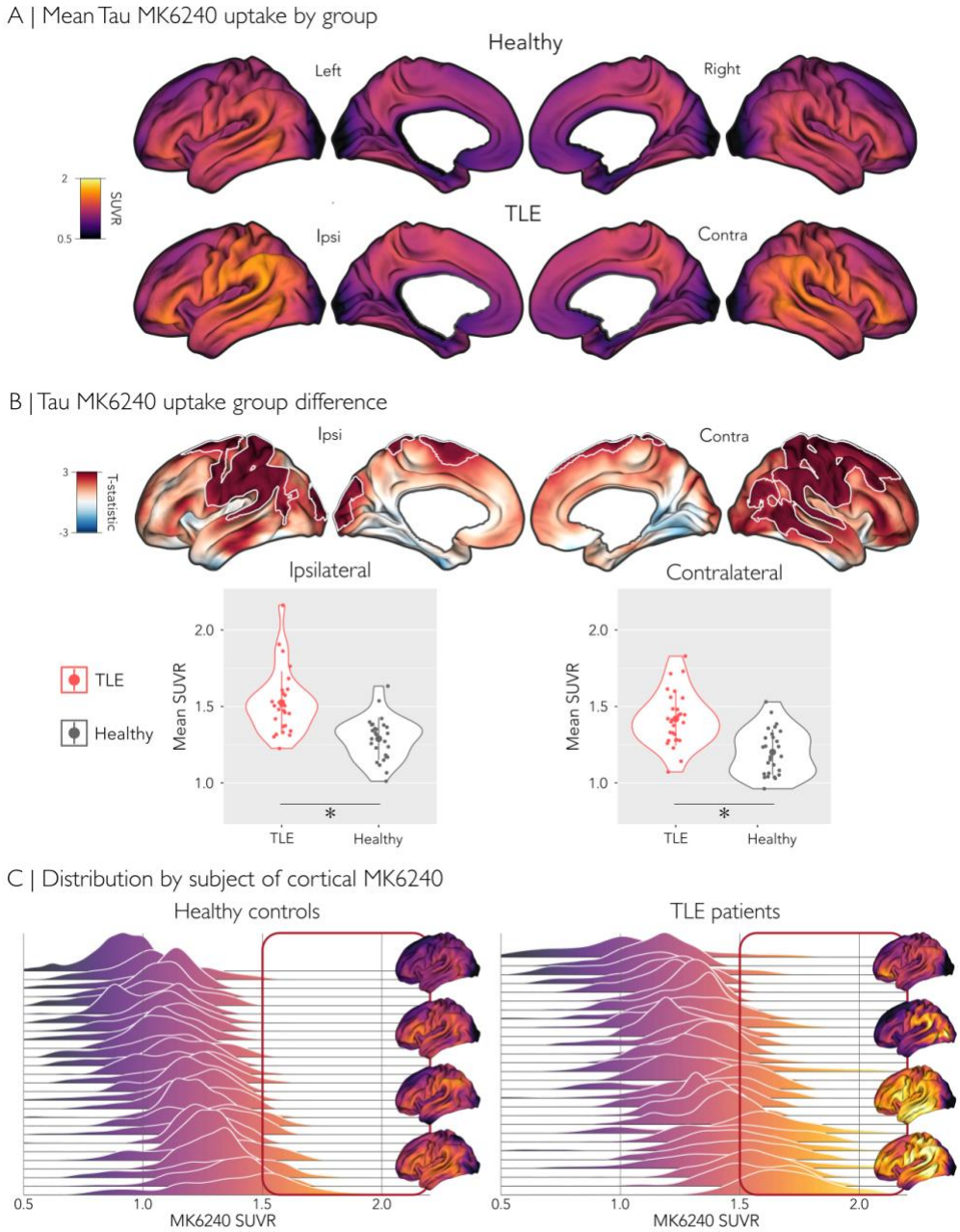

Figure 1. A) Group-Wise mean tau MK-6240 uptake. Cortical and subcortical phosphorylated tau deposits were assessed with MK-6240 and visualized as standardized uptake value ratios (SUVR). The average MK-6240 uptake is shown for healthy controls and TLE patients. **B) Group differences in MK-6240 uptake.** Group comparisons between patients and controls were performed using a mixed-effects model, adjusting for age and sex, and corrected for multiple comparisons using random field theory ($p < 0.001$). Significant regions are outlined in white. Violin plots display mean SUVR values for significant regions in each hemisphere by group, with differences assessed using a two-tailed Wilcoxon rank-sum test. **C) Subject-Wise Distribution of Cortical MK-6240 Uptake.** Density histograms illustrate the distribution of global cortical MK-6240 uptake for individual

subjects in each group. Red squares indicate regions where SUVR exceeds the abnormality threshold (SUVR > 1.5). Brain images represent individual subjects from each group with progressively increasing MK-6240 values.

Surface-wide MK-6240 SUVR findings indicated high uptake in patients relative to controls in superior-posterior temporal and parietal cortex (**Figure 1A**). Statistical comparisons based on mixed-effects models confirmed significant increases in MK-6240 SUVR between patients and controls ($p_{FWE}<0.025$, **Figure 1B**), with strongest effects localized to the ipsilateral frontal operculum and the posterior cortex, including the anterior and inferior parietal lobe (postcental, supramarginal and angular gyrus) and the lateral temporal (superior temporal gyrus) and occipital cortices. In the contralateral hemisphere, a similar pattern was observed, sparing the occipital region, but with a larger involvement of the temporal lobe, encompassing the posterior section of the superior and middle temporal gyri, and the premotor cortex . In significant clusters, we did not observe inter-hemispheric differences in overall effects (ipsilateral: $t=5.02$, $p<0.001$; contralateral: $t=4.92$, $p<0.001$).

These group-wise findings were complemented with individualized MK-6240 SUVR histogram analysis across the cortical surface (**Figure 1C**). Here, 75% of TLE patients but no controls demonstrated elevated mean SUVR above 1.5 (95th percentile), with a spatial distribution generally resembling the statistical effects. This pattern was more pronounced in the ipsilateral hemisphere but showed a similar bilateral distribution (**Supplementary Figure 1**). To assess whether MK-6240 increases were seen even after correcting for grey matter atrophy, a common feature in TLE [20,21], we re-ran the mixed effects model controlling vertex-wise for regional grey matter thickness estimates and our results were largely unaffected (**Supplementary Figure 2**).

Longitudinal data were available in a subset of our cohort (10/7 patients and 7 controls) with a minimum follow up time of 12 months (median=15 months, range=12-36 months). Although there was a numerically higher increase in MK-6240 SUVR in patients with TLE (0.0184 SUVR/year) relative to controls (0.0161 SUVR/year), this effect did not reach statistical significance (**Supplementary Figure 3**).

Association to network architecture

We assessed the overall susceptibility of globally highly interconnected regions to tauopathy using network decoding models (**Figure 2**) This analysis revealed a marginal increase in MK-6240 SUVR in highly connected regions defined by functional connectivity ($r=0.38$, $p_{spin}=0.1$), while associations with structurally connected hubs were weaker and not significant after spin tests correction ($r=0.12$, $p_{spin}=0.2$). Studying connectivity associations at the the local level (*i.e.,* association between tau uptake in a region and the connectivity strength of its immediate neighbors), there were moderate associations between regional tau SUVR and both structural ($r=0.53$, $p_{spin}<0.001$) and functional connectivity patterns ($r=0.46$, $p_{spin}=0.06$).

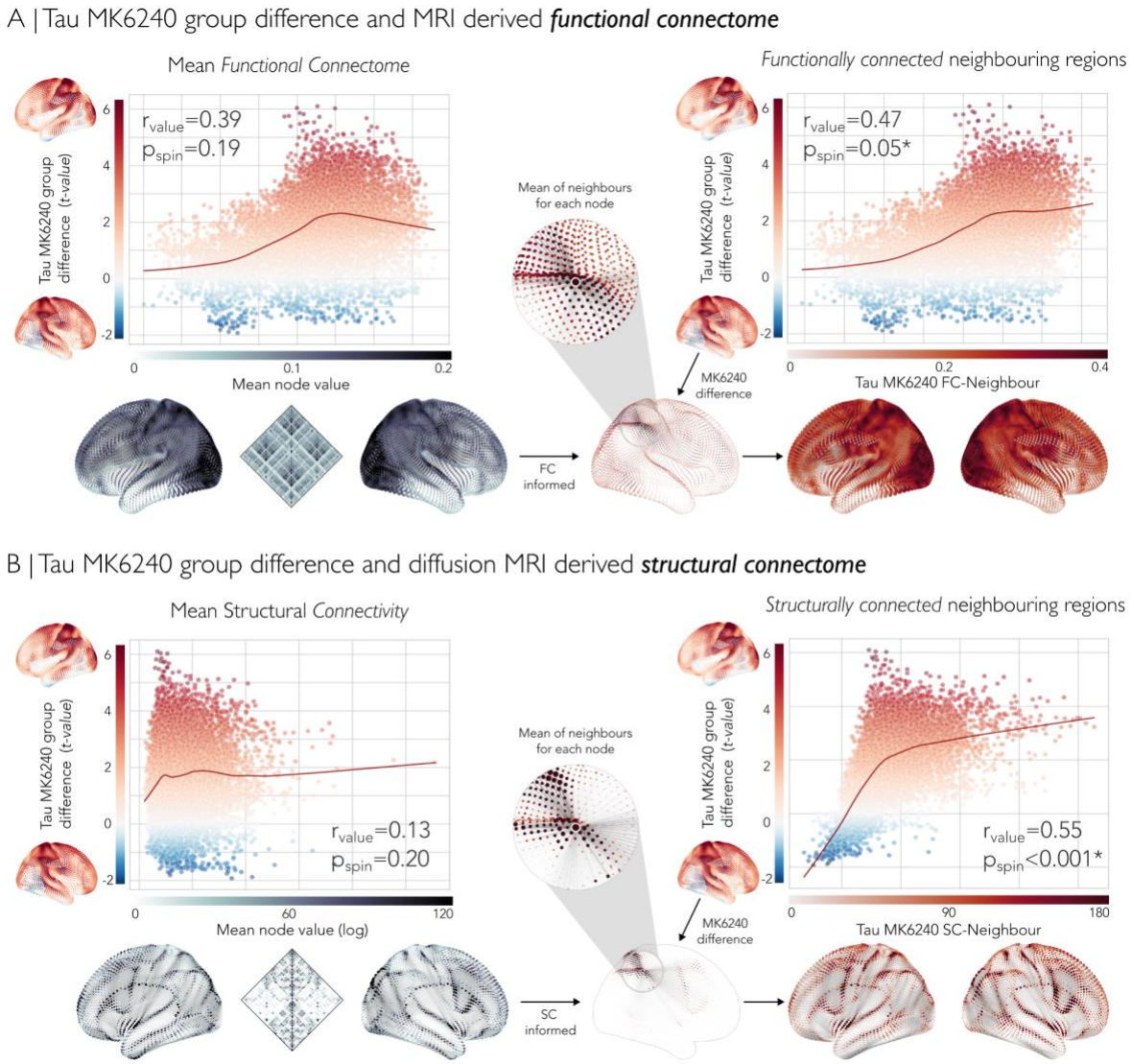

Figure 2. A) *Relationship between MK-6240 group differences and functional connectivity.* The left panel displays a scatterplot of mean node values from the functional connectome against tau MK-6240 group differences (r = 0.39, p-value =0.19). The right panel visualizes neighboring regions of each node determined by functional connectivity, with their association to tau MK-6240 group differences (r = 0.47, p-value =0.05). **B)** *Relationship between MK-6240 group differences and structural connectivity.* The structural connectome was derived from diffusion MRI tractography, and we studied its association with MK-6240 group differences. The left panel shows a logarithmic scatter plot of mean node values against group differences (r = 0.13, p-value =0.20). The right panel highlights neighboring regions based on structural connectivity, which show a strong trend of increased tau deposition (r = 0.55, p-value <0.001). The central image depicts how functional (*upper*) and structural (*lower*) connectivity informed by MK-6240 group differences was used to generate neighbor-weighted MK-6240 estimates. Points are color-coded based on MK-6240 t-values, with higher t-values indicating greater tau deposits in TLE compared to controls. The red line represents non-linear trends in the data. These findings suggest that both functional and structural network properties significantly reflected the spatial distribution of MK-6240 increases in TLE, with network hubs and their connected regions being particularly vulnerable.

Association with demographic, clinical, and cognitive measures

A weak and non-significant correlation was observed between age and mean MK-6240 SUVR (r = 0.23, p = 0.16, **Figure 3A**). In contrast, longer disease duration was significantly associated with higher MK-6240 SUVR in patients, indicating increased tau accumulation (r =

0.50, p = 0.03). This relationship was most evident in the contralateral temporal and temporo-occipital regions, as well as the ipsilateral precuneus. Notably, the duration association to tau remained consistent even after controlling for age.

We furthermore evaluated the relationship between MK-6240 and performance measures from selected cognitive tasks (**Figure 3B**). We administered the EpiTrack battery to assess executive function [22], as well as a previously validated paired associate memory paradigm to assess episodic and semantic memory [23].

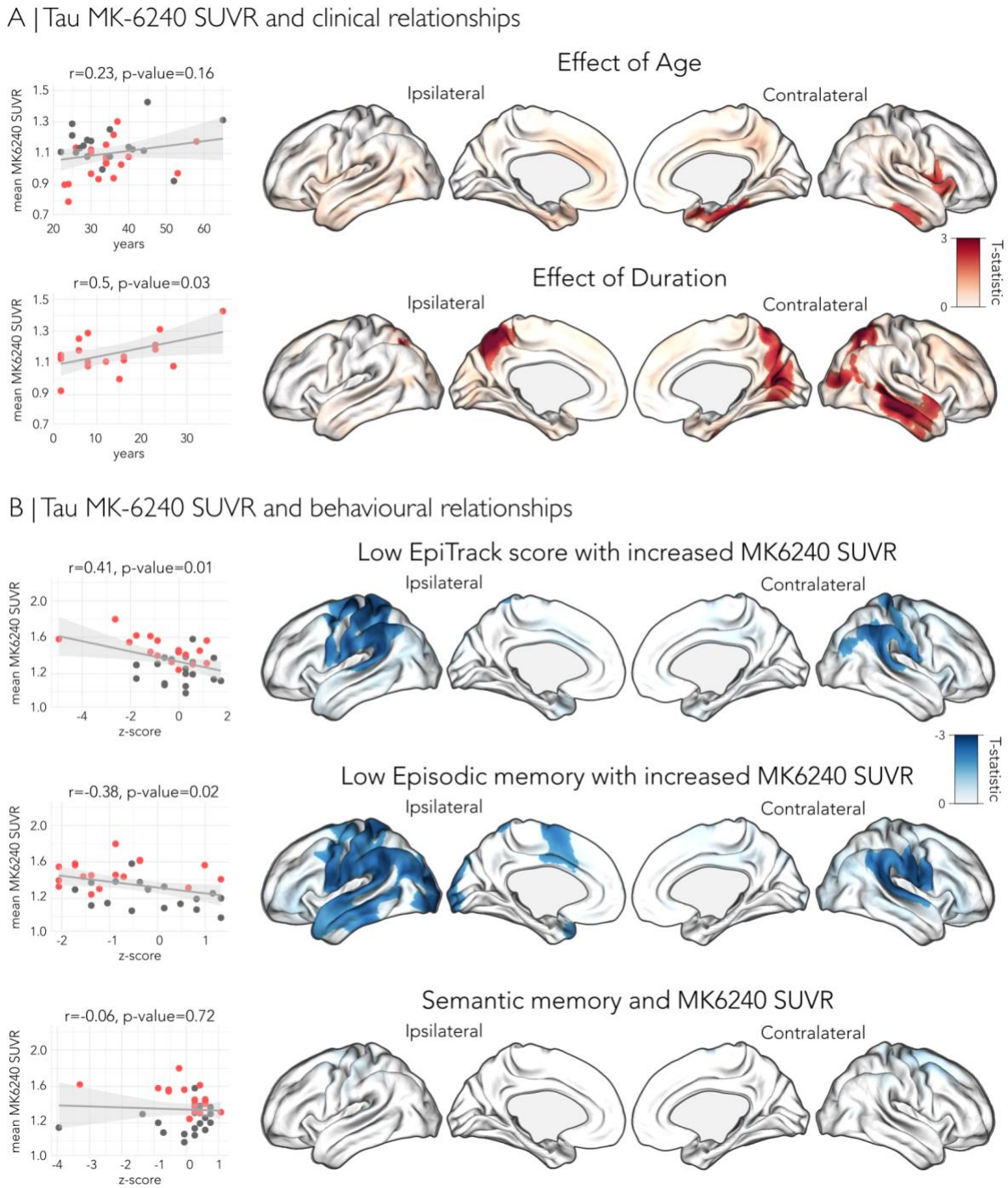

Figure 3. A) *Tau MK-6240 SUVR and clinical relationships.* Scatterplots show the association of mean MK-6240 SUVR with clinical variables. The top panel shows the relationship with age (r = 0.23, p-value = 0.16), and the

bottom panel illustrates the association with disease duration (r = 0.5, p-value = 0.03). Corresponding cortical projections visualize the regional effects of these variables on MK-6240 SUVR. Dark red on the brain maps indicate regions where age and duration are associated with increased tau deposition, as measured by t-statistics. **B)** *Tau MK-6240 SUVR and behavioral relationships.* Scatterplots display the relationship of mean MK-6240 SUVR with behavioral measures. The top panel shows the association with EpiTrack scores (r = 0.41, p-value = 0.01), the middle panel with episodic memory z-scores (r = -0.38, p-value = 0.02), and the bottom panel with semantic memory z-scores (r = -0.06, p-value = 0.72). Brain maps illustrate the corresponding regional effects, dark blue indicating areas where lower cognitive performance is associated with higher MK-6240 SUVR. Mixed-effects models were applied to assess the association between MK-6240 SUVR and these features, corrected for multiple comparisons with random field theory (p<0.01, one tail). Only significant values are highlighted; the rest are set to an alpha value of 0.2.

Cognitive performance measures revealed distinct associations with MK-6240 SUVR (**Fig. 3B**). Lower EpiTrack scores, reflecting impaired executive function, correlated with higher mean MK-6240 SUVR (r = 0.41, p = 0.01). At the vertex level, lower EpiTrack scores related to increased MK-6240 SUVR in the ipsilateral superior temporal cortex and parietal cortex (angular gyrus, somatosensory area) and in the contralateral somatosensory cortex and inferior parietal lobule. Similarly, reduced episodic memory performance showed a negative relationship with MK-6240 SUVR (r = -0.38, p = 0.02). This association was localized to similar yet more extensive areas, including the ipsilateral temporal lobe and occipital regions. In contrast, semantic memory performance did not correlate with MK-6240 SUVR (r = -0.06, p = 0.72).

DISCUSSION

This study represents the first *in-vivo* evidence of elevated phosphorylated tau, measured by [^{18}F]MK-6240 PET, in young adults with TLE compared to healthy controls, and examines its association with duration of disease, episodic memory performance, and local connectivity patterns. Tau increases showed a broad, bilateral distribution, with predominant involvement of the temporal and parietal cortices. Network-level analysis revealed moderate associations between regional tau uptake and both global mean connectivity and local structural and functional connectivity patterns. Notably, we observed more marked MK-6240 uptake in patients with longer disease duration and in those with more marked impairment in episodic memory and executive function. These findings suggest that tau accumulation may contribute to the progression of TLE and cognitive decline, supporting the potential role of tau in neurodegeneration in pharmaco-resistant epilepsy *in-vivo*.

While so far unexplored in epilepsy research, the [^{18}F]MK-6240 PET tracer has been repeatedly applied to map disease processes in established neurodegenerative conditions, in particular AD[24–26]. In those assessments, MK-6240 has been shown to generally describe the typical Braak pattern of pathological spread away from an entorhinal/mesiotemporal disease epicentre to involve bilateral, large scale networks [25–27]. Several assessments in AD have also shown that tau PET changes have associations with overall cognitive impairment and atrophy, both at the time of scanning [28,29] and prospectively [30]. These findings have been complemented with several histopathological and electron microscopic validation experiments [31], suggesting that MK-6240 does scale with the overall deposition of hyperphosphorylated tau. A key strength of this study is its focus on young and middle-aged individuals—an underexplored population in tau imaging research. Despite the younger age of the cohort, we observed a robust increase in MK-6240 binding in our patients. The observed pattern of tau deposition, involving the superior and middle temporal regions, as well as parietal-occipital areas, aligns in part with earlier *ex-vivo* observations of increased abnormalities in the ipsilateral temporal lobe relative to the epileptogenic focus [3,10,32–34], and confirms recent CSF-biomarker findings suggesting increased tau in TLE [35]. These results provide *in-vivo* evidence suggesting that TLE is associated with an elevated risk of tau-associated pathophysiological processes[36]. Crucially, we observed robust increases in tau deposition in TLE patients relative to controls after adjusting for age and sex, with findings remaining significant after correction for multiple comparisons.

Pathological validation of PET findings through post-operative immunohistochemistry will be essential for confirming *in-vivo* observations moving forward. An important consideration in interpreting the findings is the structural heterogeneity of tau fibrils across different tauopathies [37]. Tau fibrils can adopt disease-specific conformation, which in turn influence the binding properties of tau PET tracers [38]. In *ex-vivo* studies both tau isoforms 3R and 4R were confirmed in positive cases [10], yet many epilepsy cases show minimal or absent pTau. This variability suggests age-related vulnerability and the involvement of multiple, potentially distinct mechanisms [39]. Arguably while the observed findings most likely indicate overall increases in tau, findings may also co-localize with other processes thought to play a role in TLE, including inflammatory cascades. Several reports in TLE have shown associations between cortical

atrophy patterns and microglial activation as well as other inflammatory processes [40,41]. To enhance biological specificity, further studies are needed to clarify the conformation, post-translational modifications, and PET tracer binding properties of tau aggregates in epilepsy, particularly for tracers like MK-6240.

Connectome decoding models have previously been applied to describe network effects in the expression of specific imaging phenotypes, in both neurodevelopmental and neurodegenerative conditions [42–47]. In our study, we explored global as well as local connectivity associations to patient-related MK-6240 increases. While the former approach aimed to test an overall susceptibility of highly interconnected hub regions to tauopathy, the latter assessed a more local association between tau uptake and a region's connectivity patterns. Notably, while TLE-related increases in tau showed only marginal associations with global functional connectivity, stronger associations emerged with local connectivity patterns—both structurally and functionally. These findings suggest a subtle vulnerability of polysynaptic functional hubs, alongside a more pronounced influence of local network architecture. The selective susceptibility of highly connected cortical hubs in TLE has been described in studies of atrophy, and our findings extend this vulnerability to tau pathology[45]. In neurodegeneration research, local connectivity has been linked to the mechanisms of regional propagation, in which tau spreads through anatomically connected networks to affect an increasing set of brain regions [27,48,49].

We found an overall association between MK-6240 and disease duration, but not age. Disease duration was associated with a more widespread increase in MK-6240 SUVR, which may reflect tau propagation along interconnected networks rather than an age-related baseline effect [14]. This distinction highlights the potential role of disease progression in driving large-scale tau accumulation in TLE. This suggests an accumulation of tau pathology during the clinical course of TLE, emphasizing its potential role in TLE disease progression [3,50]. Of note, however, while longitudinal analysis in a subgroup of patients showed slightly higher annual increases in TLE patients relative to controls, findings were not statistically significant. Increasing the sample size—with ideally longer longitudinal follow up times and an older average age of included patients—may boost sensitivity to detect progressive tau uptake in TLE in future work. In AD, prior work has reported an increase in tau misfolding depositions over periods longer than five years and in individuals older than 65 years [51,52]. Despite these limitations, our findings also demonstrated significant associations between MK-6240 uptake and poorer performance in executive function and episodic memory, which again support a potential role of phosphorylated tau in progressive dysfunction in TLE. These findings suggest a vulnerability of cognitive networks governing episodic memory and executive function to tau-related pathology in TLE. The preservation of semantic memory in our patients and the absence of a correlation with MK-6240 may, on the other hand, suggest compensatory mechanisms similar to those in AD, where episodic memory and executive function are more markedly affected than semantic memory and conceptual knowledge [53,54,3].

Together, these findings suggest that elevated phosphorylated tau in young adults with TLE may represent a candidate mechanism contributing to progressive network dysfunction. As tau imaging in epilepsy advances, integrating larger, longitudinal, and multimodal datasets across

diverse age ranges will be critical to clarifying disease trajectories and individual variability. Ultimately, this work lays the groundwork for a network-based molecular framework of epilepsy, which can be refined as more high-resolution *in-vivo* and *post-mortem* data become available.

METHODS

PARTICIPANTS

We recruited 18 TLE patients (6 Females, mean±SD age=34.6±10.1 years) and 20 healthy volunteers with a similar age and sex distribution (6 Females, mean±SD age=34.6±7.6 years) between May 2018 and November 2024. Diagnosis of TLE and lateralization of seizure foci were determined by the criteria of the International League Against Epilepsy (ILAE), based on a comprehensive examination that included clinical history, neurological examination, review of medical records, video-electroencephalography (EEG) recordings, and clinical MRI. As in earlier work [55], hippocampal atrophy was determined as volumes or left-right asymmetry beyond 2 standard deviations of the corresponding mean of healthy controls: 7 patients had unilateral hippocampal atrophy ipsilateral to the focus and 11 had normal hippocampal volume. No control had hippocampal atrophy according to these criteria. Mean±SD age at seizure onset was 22±13 years and mean±SD duration of epilepsy was 13±10 years. Healthy controls were recruited via advertisement; all denied a history of neurological, psychiatric, or significant medical comorbidities, including traumatic brain injury. A subgroup in both cohorts had longitudinal acquisition (10/7 patients and 7 controls) with a minimum follow up time of 12 months(median=15 months, range=12 months - 3 years).

STANDARD PROTOCOL APPROVALS, REGISTRATIONS, AND PATIENT CONSENTS

The Ethics Committee of the Montreal Neurological Institute and Hospital (MNI) approved the study (#2018-4148). Written informed consent, including a statement for open sharing of collected research data, was obtained from all participants.

PET IMAGE ACQUISITION AND PROCESSING

Tau PET scanning was performed on a Siemens high-resolution research tomograph (HRRT) at the McConnell Brain Imaging Center of the MNI, using [^{18}F]-MK-6240 tracer[17], which shows low off-target binding[16]. The tracer was injected intravenously, and images were acquired after 90 minutes for approximately 30 minutes. A previous validation study in our center has shown that scans 90-110 minutes post-injection may optimally balance duration and signal[56]. In TLE, mean injected MK-6240 activity was 244.2±25.9 MBq/L. In controls, it was 236.8±40.7 MBq/L. Images were reconstructed with an ordered subset expectation maximization algorithm. A short transmission scan (11 minutes) with a rotating Cesium137 source was used for attenuation correction and later for co-registration to participant-specific MRI data. Images underwent correction for dead time, decay, as well as random and scattered coincidences. Dynamic MK-6240 images (4 in total) were co-registered and averaged. Average MK-6240 uptake was registered with an affine transformation to processed T1-weighted MRI (T1w) data (see below, and **Supplementary Figure 5**). Next, it was partial volume corrected using a probabilistic mask of the grey matter. We calculated standardized uptake value ratio

(SUVR) images using the cerebellar grey matter as a reference region[56]. To assess reproducibility in the mixed effects models, we additionally tested the use of the brainstem and a composite reference region **Supplementary Figure 6** [57]. The SUVR volume was registered to the medial cortical surface derived from T1-weighted MRI, resulting in surface-based MK-6240 maps. Surface-based MK-6240 data were blurred with a 10-mm FWHM surface-based kernel, and participant-specific data were re-sampled to the fsLR-32k template surface[58].

MULTIMODAL MRI ACQUISITION AND PROCESSING

MRI scans were also obtained at the McConnell Brain Imaging Centre, using a 3T Siemens Magnetom Prisma-Fit scanner equipped with a 64-channel head coil. Participants underwent a T1w structural scan, followed by multi-shell diffusion weighted imaging (DWI) and resting-state functional MRI (rs-fMRI). T1w images were acquired using a 3D-MPRAGE sequence (0.8 mm isovoxels). Diffusion-weighted imaging data were collected using a multi-band accelerated 2D spin-echo EPI sequence (1.6 mm isovoxels) with three b-value shells (300, 700, 2000 s/mm²) and corresponding diffusion directions (10, 40, 90), along with phase-reversed b0 images for distortion correction. rs-fMRI scans were acquired with a 7-min multiband 2D-BOLD EPI sequence (3 mm isovoxels, TR = 600 ms), with participants instructed to keep their eyes open and fixate on a cross. For detailed parameters, see [59].

Multimodal MRI data processing and feature fusion leveraged micapipe v0.2.3 (http://micapipe.readthedocs.io), with details described elsewhere [60]. In brief, T1w data were processed for intensity abnormalities, followed by automated segmentation of subcortical structures using FSL FIRST [53], the generation of probabilistic tissue estimates using FSL FAST [61], and cortical surface segmentations using FreeSurfer 6.0 [62]. Surfaces were manually quality controlled and corrected if necessary. This was complemented with structural connectome (SC) generation based on diffusion-weighted MRI data, and functional connectome (FC) generation based on rs-fMRI time series. SC generation succeeded standard diffusion MRI preprocessing, which involved motion correction, denoising, and correction for inhomogeneity and geometric distortions. Anatomically constrained tractography was performed using tissue segmentations derived from each participant's T1w images that were co-registered to native diffusion space. Multi-shell and multi-tissue response functions were estimated, followed by constrained spherical deconvolution and intensity normalization. A tractogram with 40M streamlines was generated and refined using SIFT2 [63]. Connection weights are defined as the weighted streamline counts between nodes mapped to the Schaefer-200 parcellation [64]. A second connectome used edge length as the connection weights. Finally, both measures were combined to create a weighted structural connectome (SCw) that integrates connectivity and distance information. Functional MRI processing involved motion and distortion correction, denoising, bandpass filtering, and surface registration. fMRI time-series were then averaged within Schaefer-200 cortical parcels, and FC estimated from Fisher-R-to-Z transformed cross-correlation matrices.

STATISTICAL ANALYSIS

Analyses were performed using BrainStat[65], an open-access toolbox for brain-wide statistical analysis (http://brainstat.readthedocs.io). In patients, prior to analysis, cortical features were sorted into ipsilateral/contralateral relative to the seizure focus.

a) Mapping of tau uptake in TLE. We compared MK-6240 vertex-wise SUVR between individuals with TLE and healthy controls using a surface-based linear mixed effects model, controlling for age, sex, and participant as a random effect. In addition to examining between-group differences, we evaluated whether within-subject longitudinal trajectories of MK-6240 SUVR differed between patients and controls using interaction models. Statistical between-group comparisons were complemented by individualized mapping of cortical areas with a high probability of MK-6240 SUVR >1.5; defined as the 95nd percentile in healthy subjects.

b) Network contextualization. We correlated the *t*-statical map from analysis a) with network metrics derived from SC and FC. Specifically, network metrics were mean connectivity and neighborhood-weighted connectivity [66]. To minimize confounding effects, medial wall vertices were excluded from the connectome matrices in all calculations, and spin tests were performed using 10,000 permutations to assess statistical significance while accounting for spatial autocorrelation [67,68].

c) Relationship to clinical and cognitive variables. We correlated global and vertex-wise SUVR data to age and disease duration, as well as cognitive measures obtained outside of the PET scanner. Cognitive assessment included the EpiTrack, a brief 15-minute screening tool designed to detect and monitor cognitive side effects of antiepileptic drugs (AEDs) and the adverse effects of seizures in patients with epilepsy. Episodic and semantic memory were also assessed using standardized tasks: the episodic memory task involved learning and recalling object pairs across encoding and retrieval phases, while the semantic memory task required identifying conceptually related object pairs from visual prompts.[22,23]. TLE patients showed lower performance on the episodic memory task (t=2.53, p=0.016), while performance did not differ from controls for the EpiTrack (t=1.73, p=0.09) and the semantic memory task (t=-0.05, p=0.96). Analyses contrived for age.

d) Control for multiple comparisons. Findings were corrected for multiple comparisons with random field theory, two tails for the SUVR comparison between TLE and healthy subjects ($p < 0.001$), and one tail for the vertex-wise SUVR one direction correlation with clinical and cognitive variables ($p<0.05$).

DATA AVAILABILITY

All the data used in the study will be found on OSF upon publication of this work (https://osf.io/ct3gw) .

CODE AVAILABILITY

All processing workflow scripts and the code for analyses and statistics are openly available on GitHub (https://github.com/MICA-MNI/2025_in-vivo_tauPET-mk6240_TLE).

ACKNOWLEDGEMENTS

We thank the McConnell Brain Imaging Centre (BIC) PET and MRI units of the MNI, and the study participants for supporting our research. RRC received support from the Fonds de la Recherche du Québec – Santé (FRQ-S), the Montreal Neurological Institute Jeanne Timmins Costello Fellowship, and the Healthy Brains, Healthy Lives – Entrepreneur Postdoc Fellowship. JR received support from the Canadian Open Neuroscience Platform (CONP) and Canadian Institutes of Health Research (CIHR). MK is supported by the Wellcome Trust (221934/Z/20/Z). LC acknowledges previous support from Brain Research UK (Award 14181). BCB acknowledges support from CIHR (FDN-154298, PJT-174995), SickKids Foundation (NI17-039), Natural Sciences and Engineering Research Council (NSERC; Discovery-1304413), Azrieli Center for Autism Research of the Montreal Neurological Institute (ACAR), BrainCanada, FRQ-S, the Helmholtz International BigBrain Analytics and Learning Laboratory (Hiball), the Canada Research Chairs Program (CRC), and the Centre of Excellence in Epilepsy at the Neuro (CEEN).

REFERENCES

1. Pitkänen, A. & Sutula, T. P. Is epilepsy a progressive disorder? Prospects for new therapeutic approaches in temporal-lobe epilepsy. Lancet Neurol. 1, 173–181 (2002).
2. Galovic, M. et al. Progressive Cortical Thinning in Patients With Focal Epilepsy. JAMA Neurol 76, 1230–1239 (2019).
3. Tai, X. Y. et al. Review: Neurodegenerative processes in temporal lobe epilepsy with hippocampal sclerosis: Clinical, pathological and neuroimaging evidence. Neuropathol. Appl. Neurobiol. 44, 70–90 (2018).
4. Caciagli, L. et al. A meta-analysis on progressive atrophy in intractable temporal lobe epilepsy: Time is brain? Neurology 89, 506–516 (2017).
5. Boyle, P. A., Wilson, R. S., Aggarwal, N. T., Tang, Y. & Bennett, D. A. Mild cognitive impairment. Neurology 67, 441–445 (2006).
6. Noebels, J. A perfect storm: Converging paths of epilepsy and Alzheimer's dementia intersect in the hippocampal formation. Epilepsia 52 Suppl 1, 39–46 (2011).
7. Association of Seizure Foci and Location of Tau and Amyloid Deposition and Brain Atrophy in Patients With Alzheimer Disease and Seizures. Neurology 104, e210173 (2025).
8. Irizarry, M. C. et al. Incidence of new-onset seizures in mild to moderate Alzheimer disease. Arch. Neurol. 69, 368–372 (2012).
9. Amatniek, J. C. et al. Incidence and predictors of seizures in patients with Alzheimer's disease. Epilepsia 47, 867–872 (2006).
10. Tai, X. Y. et al. Hyperphosphorylated tau in patients with refractory epilepsy correlates with cognitive decline: a study of temporal lobe resections. Brain 139, 2441–2455 (2016).
11. Salemme, S. et al. The prognosis of mild cognitive impairment: A systematic review and meta-analysis. Alzheimers Dement (Amst) 17, e70074 (2025).
12. Canet, G. et al. Seizure activity triggers tau hyperphosphorylation and amyloidogenic pathways. Epilepsia 63, 919–935 (2022).
13. Alves, M., Kenny, A., de Leo, G., Beamer, E. H. & Engel, T. Tau Phosphorylation in a Mouse Model of Temporal Lobe Epilepsy. Front. Aging Neurosci. 11, 490080 (2019).
14. Thom, M. & Koepp, M. Tau protein in drug-resistant epilepsy and cognitive decline. in Inflammation and Epilepsy: New Vistas 149–184 (Springer International Publishing, Cham, 2021).
15. Malarte, M.-L., Nordberg, A. & Lemoine, L. Characterization of MK6240, a tau PET tracer, in autopsy brain tissue from Alzheimer's disease cases. Eur. J. Nucl. Med. Mol. Imaging 48, 1093–1102 (2021).
16. Aguero, C. et al. Autoradiography validation of novel tau PET tracer [F-18]-MK-6240 on human postmortem brain tissue. Acta Neuropathologica Communications 7, 1–15 (2019).
17. Hopewell, R. et al. A simplified radiosynthesis of [F]MK-6240 for tau PET imaging. J Labelled Comp Radiopharm 62, 109–114 (2019).
18. Knowlton, R. C. et al. In vivo hippocampal glucose metabolism in mesial temporal lobe epilepsy. Neurology 57, 1184–1190 (2001).
19. Juhász, C. et al. Glucose and [11C]flumazenil positron emission tomography abnormalities of thalamic nuclei in temporal lobe epilepsy. Neurology 53, 2037–2045 (1999).
20. Kerestes, R. et al. Patterns of subregional cerebellar atrophy across epilepsy syndromes: An ENIGMA-Epilepsy study. Epilepsia 65, 1072–1091 (2024).
21. Whelan, C. D., Haaker, J. G. & Sisodiya, S. M. Structural Brain Abnormalities in the Common Epilepsies Assessed in a Worldwide ENIGMA Study. (2018).
22. Lutz, M. T. & Helmstaedter, C. EpiTrack: tracking cognitive side effects of medication on attention and executive functions in patients with epilepsy. Epilepsy Behav 7, 708–714 (2005).

23. Cabalo, D. G. et al. Differential reorganization of episodic and semantic memory systems in epilepsy-related mesiotemporal pathology. Brain 147, 3918–3932 (2024).
24. Betthauser, T. J. et al. In Vivo Characterization and Quantification of Neurofibrillary Tau PET Radioligand 18F-MK-6240 in Humans from Alzheimer Disease Dementia to Young Controls. Journal of Nuclear Medicine 60, 93–99 (2019).
25. Pascoal, T. A. et al. 18F-MK-6240 PET for early and late detection of neurofibrillary tangles. Brain 143, 2818–2830 (2020).
26. Kreisl, W. C. et al. Patterns of tau pathology identified with 18F-MK-6240 PET imaging. Alzheimer's & Dementia 18, 272–282 (2022).
27. Pascoal, T. A. et al. Longitudinal 18F-MK-6240 tau tangles accumulation follows Braak stages. Brain 144, 3517–3528 (2021).
28. Malpetti, M., La Joie, R. & Rabinovici, G. D. Tau Beats Amyloid in Predicting Brain Atrophy in Alzheimer Disease: Implications for Prognosis and Clinical Trials. Journal of Nuclear Medicine 63, 830–832 (2022).
29. Ossenkoppele, R. et al. Accuracy of Tau Positron Emission Tomography as a Prognostic Marker in Preclinical and Prodromal Alzheimer Disease: A Head-to-Head Comparison Against Amyloid Positron Emission Tomography and Magnetic Resonance Imaging. JAMA Neurol 78, 961–971 (2021).
30. La Joie, R. et al. Prospective longitudinal atrophy in Alzheimer's disease correlates with the intensity and topography of baseline tau-PET. Sci. Transl. Med. 12, (2020).
31. Kunach, P. et al. Cryo-EM structure of Alzheimer's disease tau filaments with PET ligand MK-6240. Nat Commun 15, 8497 (2024).
32. Gourmaud, S. et al. Alzheimer-like amyloid and tau alterations associated with cognitive deficit in temporal lobe epilepsy. Brain 143, 191–209 (2020).
33. Smith, K. M. et al. Tau deposition in young adults with drug-resistant focal epilepsy. Epilepsia 60, 2398–2403 (2019).
34. Thom, M. et al. Neurofibrillary tangle pathology and Braak staging in chronic epilepsy in relation to traumatic brain injury and hippocampal sclerosis: a post-mortem study. Brain 134, 2969–2981 (2011).
35. Ballerini, A. et al. Late-onset temporal lobe epilepsy: insights from brain atrophy and Alzheimer's disease biomarkers. Brain 148, 185–198 (2025).
36. Bernasconi, N. Is epilepsy a curable neurodegenerative disease? Brain 139, 2336–2337 (2016).
37. Vaquer-Alicea, J., Diamond, M. I. & Joachimiak, L. A. Tau strains shape disease. Acta Neuropathol 142, 57–71 (2021).
38. Groot, C., Villeneuve, S., Smith, R., Hansson, O. & Ossenkoppele, R. Tau PET Imaging in Neurodegenerative Disorders. J Nucl Med 63, 20S–26S (2022).
39. Mrzyglod, A. et al. Patterns of phosphorylated tau accumulation in a spectrum of acquired and developmental brain lesions associated with refractory epilepsy. Epilepsia (2025) doi:10.1111/epi.18418.
40. Altmann, A. et al. A systems-level analysis highlights microglial activation as a modifying factor in common epilepsies. Neuropathol Appl Neurobiol 48, e12758 (2022).
41. Dickstein, L. P. et al. Neuroinflammation in neocortical epilepsy measured by PET imaging of translocator protein. Epilepsia 60, 1248–1254 (2019).
42. Seeley, W. W., Crawford, R. K., Zhou, J., Miller, B. L. & Greicius, M. D. Neurodegenerative diseases target large-scale human brain networks. Neuron 62, 42–52 (2009).
43. Zhou, J., Gennatas, E. D., Kramer, J. H., Miller, B. L. & Seeley, W. W. Predicting regional neurodegeneration from the healthy brain functional connectome. Neuron 73, 1216–1227 (2012).

44. Crossley, N. A. et al. The hubs of the human connectome are generally implicated in the anatomy of brain disorders. Brain 137, 2382–2395 (2014).
45. Larivière, S. et al. Network-based atrophy modeling in the common epilepsies: A worldwide ENIGMA study. Sci Adv 6, (2020).
46. Royer, J. et al. Epilepsy and brain network hubs. Epilepsia 63, 537–550 (2022).
47. Georgiadis, F. et al. Connectome architecture shapes large-scale cortical alterations in schizophrenia: a worldwide ENIGMA study. Mol Psychiatry 29, 1869–1881 (2024).
48. Liu, L. et al. Trans-synaptic spread of tau pathology in vivo. PLoS One 7, e31302 (2012).
49. Braak, H., Alafuzoff, I., Arzberger, T., Kretzschmar, H. & Del Tredici, K. Staging of Alzheimer disease-associated neurofibrillary pathology using paraffin sections and immunocytochemistry. Acta Neuropathol 112, 389–404 (2006).
50. Sánchez, M. P., García-Cabrero, A. M., Sánchez-Elexpuru, G., Burgos, D. F. & Serratosa, J. M. Tau-Induced Pathology in Epilepsy and Dementia: Notions from Patients and Animal Models. Int J Mol Sci 19, (2018).
51. Harrison, T. M. et al. Longitudinal tau accumulation and atrophy in aging and alzheimer disease. Ann Neurol 85, 229–240 (2019).
52. Pan, N., Liu, S., Ge, X., Zheng, Y. & for Alzheimer's Disease Neuroimaging Initiative. Association of hippocampal atrophy with tau pathology of temporal regions in preclinical Alzheimer's disease. J Alzheimers Dis 13872877251314785 (2025).
53. Patenaude, B., Smith, S. M., Kennedy, D. N. & Jenkinson, M. A Bayesian model of shape and appearance for subcortical brain segmentation. Neuroimage 56, 907–922 (2011).
54. Perceptual and semantic contributions to episodic memory: evidence from semantic dementia and Alzheimer's disease. Journal of Memory and Language 47, 197–213 (2002).
55. Bernhardt, B. C. et al. Temporal lobe epilepsy: Hippocampal pathology modulates connectome topology and controllability. Neurology 92, e2209–e2220 (2019).
56. Pascoal, T. A. et al. In vivo quantification of neurofibrillary tangles with [F]MK-6240. Alzheimers. Res. Ther. 10, 74 (2018).
57. Landau, S. M. et al. Measurement of longitudinal β-amyloid change with 18F-florbetapir PET and standardized uptake value ratios. J Nucl Med 56, 567–574 (2015).
58. Van Essen, D. C., Glasser, M. F., Dierker, D. L., Harwell, J. & Coalson, T. Parcellations and hemispheric asymmetries of human cerebral cortex analyzed on surface-based atlases. Cereb. Cortex 22, 2241–2262 (2012).
59. Royer, J. et al. An Open MRI Dataset For Multiscale Neuroscience. Sci Data 9, 569 (2022).
60. Cruces, R. R. et al. Micapipe: A pipeline for multimodal neuroimaging and connectome analysis. Neuroimage 263, 119612 (2022).
61. Zhang, Y., Brady, M. & Smith, S. Segmentation of brain MR images through a hidden Markov random field model and the expectation-maximization algorithm. IEEE Trans. Med. Imaging 20, 45–57 (2001).
62. Fischl, B. FreeSurfer. Neuroimage 62, 774–781 (2012).
63. Tournier, J.-D. et al. MRtrix3: A fast, flexible and open software framework for medical image processing and visualisation. Neuroimage 202, 116137 (2019).
64. Schaefer, A. et al. Local-Global Parcellation of the Human Cerebral Cortex from Intrinsic Functional Connectivity MRI. Cereb Cortex 28, 3095–3114 (2018).
65. Larivière, S. et al. BrainStat: A toolbox for brain-wide statistics and multimodal feature associations. Neuroimage 266, 119807 (2023).
66. Shafiei, G. et al. Spatial Patterning of Tissue Volume Loss in Schizophrenia Reflects Brain Network Architecture. Biol Psychiatry 87, 727–735 (2020).

67. Vos de Wael, R. et al. BrainSpace: a toolbox for the analysis of macroscale gradients in neuroimaging and connectomics datasets. Commun Biol 3, 103 (2020).
68. Alexander-Bloch, A. F. et al. On testing for spatial correspondence between maps of human brain structure and function. Neuroimage 178, 540–551 (2018).

AUTHOR INFORMATION

Authors and affiliations

McConnell Brain Imaging Centre, Montreal Neurological Institute, McGill University, Montreal, Québec, Canada.
Raúl R. Cruces, Jack Lam, Thaera Arafat, Jessica Royer, Judy Chen, Ella Sahlas, Robert Hopewell, Chris Hung-Hsin Hsiao, Gassan Massarweh, Jean-Paul Soucy, Andrea Bernasconi, Neda Bernasconi, Boris C. Bernhardt**
* joint senior authors

Montreal Neurological Institute, McGill University Health Centre (MUHC) and other McGill University
Raluca Pana

StoP-AD Centre, Douglas Mental Health University Institute, McGill University, Montréal, QC, Canada
Sylvia Villeneuve

UCL Queen Square Institute of Neurology, University College London, London WC1N 3BG, UK
Matthias Koepp

Department of Neurology, Inselspital, Sleep-Wake-Epilepsy Center, Bern University Hospital, University of Bern, Bern, Switzerland
Lorenzo Caciagli

Corresponding authors

Raul Cruces, PhD, Boris C. Bernhardt, PhD

SUPPLEMENTARY INFORMATION

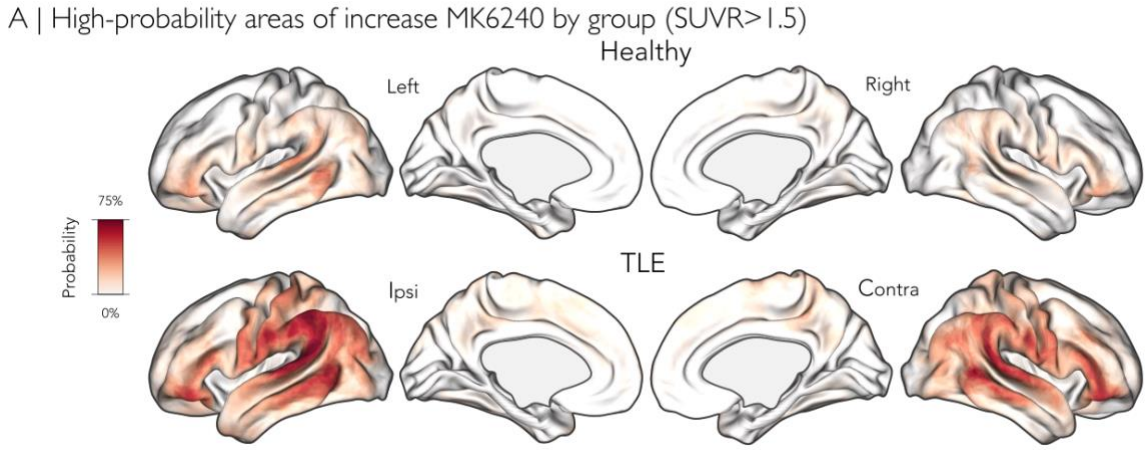

Supplementary Figure 1. Cortical map of abnormal MK-6240 SUVR probability. Regions with SUVR values greater than 1.5 were identified and visualized for each group. Dark red represents areas with higher prevalence of abnormal SUVR uptake, light red indicates lower prevalence. The maximum MK-6240 SUVR probability is in 75% of the TLE population.

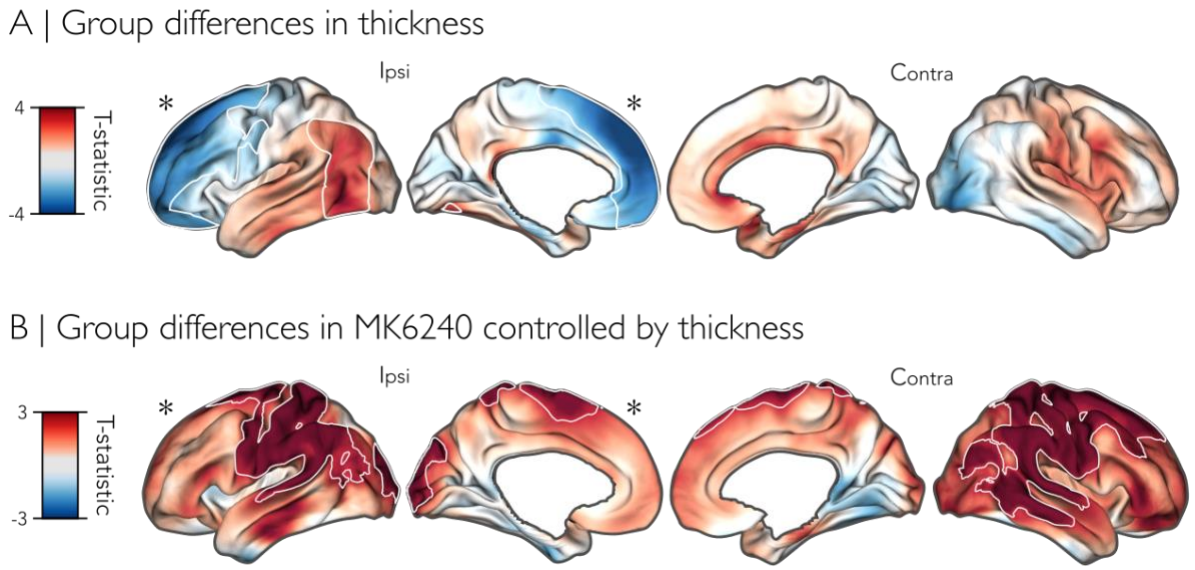

Supplementary Figure 2. A) Group difference in cortical thickness. The comparison was evaluated using a mixed effects model, controlling for age and sex, and corrected for multiple comparisons with random field theory ($p<0.001$). **B)** MK-6240 uptake comparing TLE and healthy controls after controlling for cortical thickness, using a mixed effects model, controlling for age and sex, and corrected for multiple comparisons with random field theory ($p<0.001$). Significant regions are outlined in white.

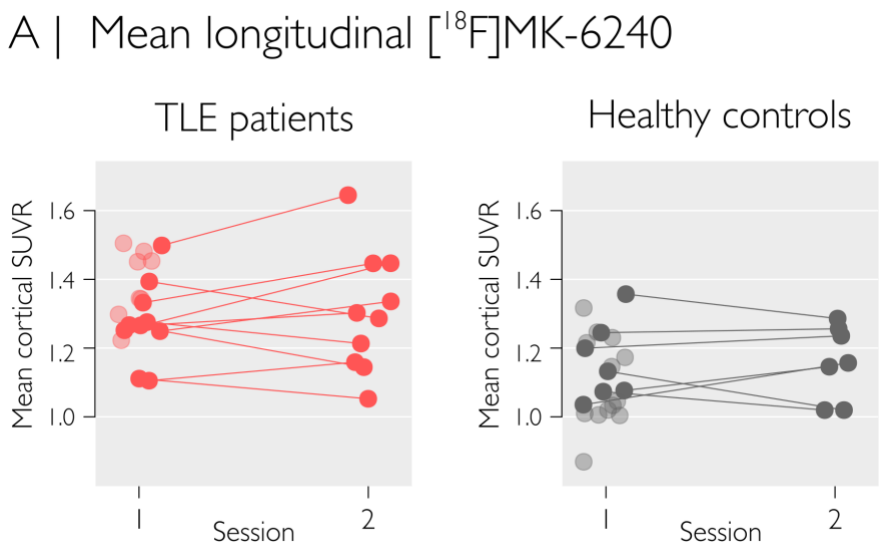

Supplementary Figure 3. Differential trajectories of [F^{18}]MK-6240 uptake by group between the PET scan session 1 and 2. The lines correspond to the longitudinal subjects.

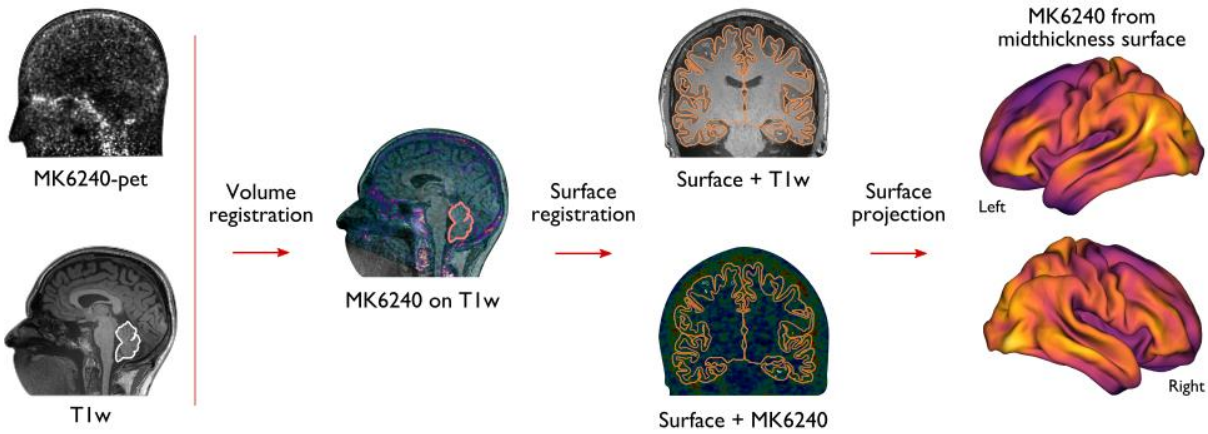

Supplementary Figure 4. Workflow of co-registration between the structural T1w MRI and the MK-6240 PET image. Normalization by the cerebellar mean SUVR and mapping to the mid-thickness surface of each subject. The right image shows an example of one subject MK-6240 map projected on a standardized surface, fsLR-32k.

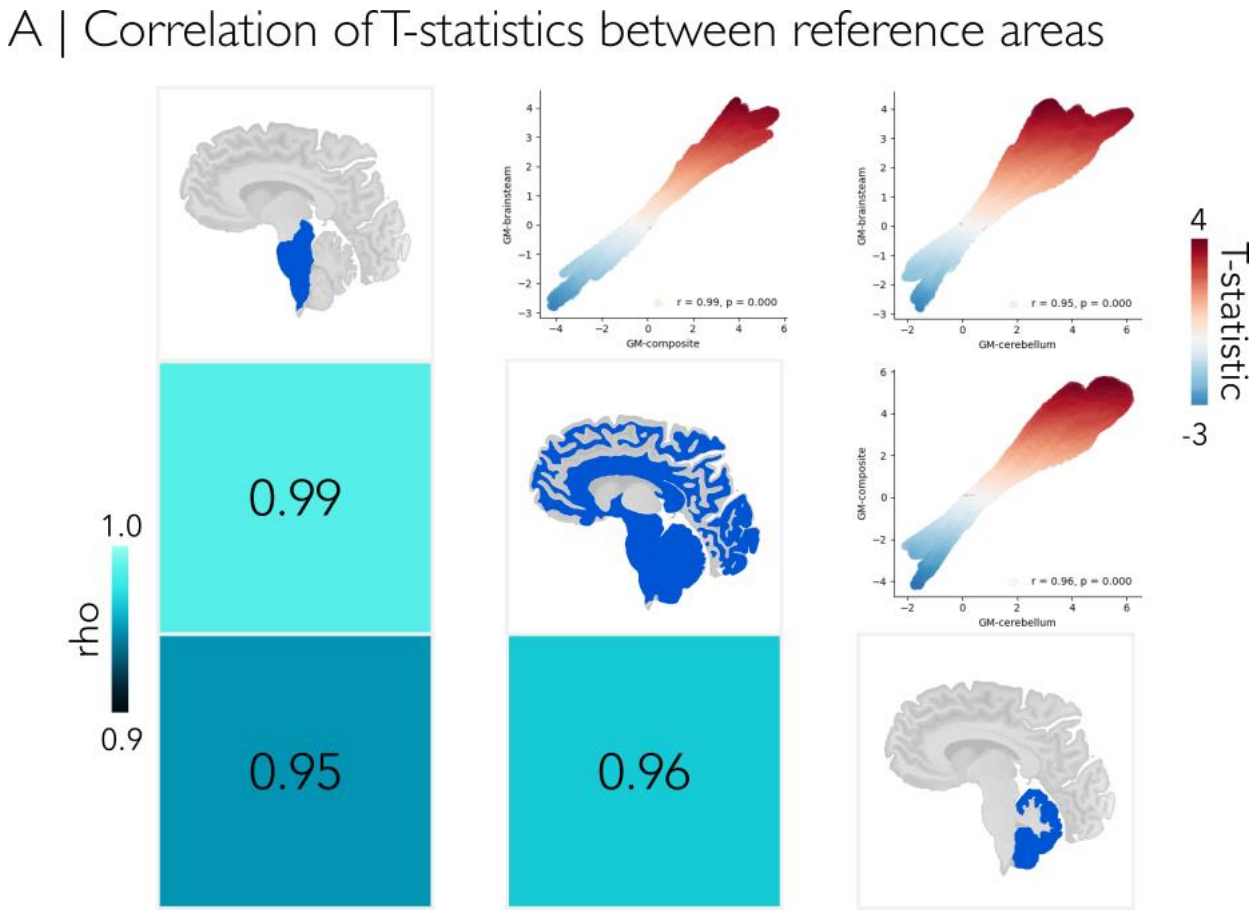

Supplementary Figure 5. Correlation of t-statistics of the between-group difference maps across different SUVR reference regions for brainstem, cerebellar gray matter (GM-cerebellum), and a composite reference. Top right scatter plots show vertex-wise t-statistics comparisons across reference choices, each with corresponding Pearson's correlation coefficients (r), demonstrating high consistency across methods ($r \geq 0.95$). Blue shaded brain maps illustrate the respective reference regions. Bottom left matrix shows Spearman's rho values between comparisons, ranging from 0.95 to 0.99. Overall, the results indicate strong agreement in regional T-statistics across different reference region choices used for MK-6240 SUVR computation.